Influence of a perfluorohexane-enriched atmosphere on the viscoelasticity and structural order of self-assembled nanodomains of semifluorinated alkanes at the air/water interface

Salomé Mielke, Wasim Abuillan, Mariam Veschgini, Xianhe Liu, Oleg Konovalov, Marie Pierre Krafft, Motomu Tanaka

Influence of a perfluorohexane-enriched atmosphere on the viscoelasticity and structural order of self-assembled nanodomains of semifluorinated alkanes at the air/water interface

Salomé Mielke[1], Wasim Abuillan[1#], Mariam Veschgini[1], Xianhe Liu[2], Oleg Konovalov[3], Marie Pierre Krafft[2*], and Motomu Tanaka[1,4*]

[1] Physical Chemistry of Biosystems, Institute of Physical Chemistry, Heidelberg University, 69120 Heidelberg, Germany

[2] University of Strasbourg, Institut Charles Sadron (CNRS), 23 rue du Loess, 67034 Strasbourg Cedex, France

[3] European Synchrotron Radiation Facility (ESRF), Grenoble Cedex 9 38053, France

[4] Center for Integrative Medicine and Physics, Institute for Advanced Study, Kyoto University, Kyoto 606-8501, Japan

[#]present address: Institute of Industrial Science, The University of Tokyo, 153-0041 Tokyo, Japan

* Corresponding Authors: krafft@unistra.fr, tanaka@uni-heidelberg.de

Abstract

Semifluorinated alkanes are promising candidates to stabilize microbubbles enriched with a fluorocarbon gas for sonographic imaging, since they form highly uniform, mesoscopic domains with the diameter of several tens of nm by self-assembly at the air/water interface. In this study, we investigated how an atmosphere enriched with a fluorocarbon gas (perfluorohexane) influences the interfacial viscoelasticity and structural order of semifluorinated alkane domains by the combination of dilational rheology and grazing incidence small-angle X-ray scattering (GISAXS) at the air/water interface. The elastic modulus of semifluorinated alkane monolayers was several times larger compared to those of surfactants with hydrocarbon segments, which can be attributed to strong dipole repulsions originating from the CF_3 termini and CF_2-CH_2 junction. The presence of perfluorohexane in the atmosphere led to a distinct decrease in the elasticity, which can be correlated to an increase in the lateral compressibility observed by pressure-area isotherms. The interfacial viscosity of semifluorinated alkane monolayers calculated from the Kelvin-Voigt model was by two orders of magnitude lower than those of surfactants with hydrocarbon segments due to the much weaker cohesion between the fluorocarbon segments. We analyzed GISAXS results by the full calculation of structure and form factors, and found that the hemispherical, about 30 nm large domains of semifluorinated alkanes form hexagonal lattices both in air and in the atmosphere enriched with perfluorohexane. Intriguingly, the presence of perfluorohexane barely influences the domain size or the distance between neighboring domains, indicating that perfluorohexane molecules do not intercalate into the fluorocarbon regions of the domains but adsorb weakly to the free spaces between the domains. Thus, the combination of dilational rheology and quantitative GISAXS is straightforward for the optimization of membrane, bubble, and emulsion systems by fine-tuning of molecular structures. These studies demonstrate the sturdiness of the self-assembled semifluorinated alkane domains that can retain the structural integrity in the presence of fluorocarbon gas.

Introduction

Perfluorocarbon compounds have been draining increasing attentions because of their unique physical and chemical properties,[1-3] owing to the extremely low polarizability of fluorine.[2] The strong C-F bond makes fluorocarbon compounds very stable compared to hydrocarbon compounds. The low polarizability of fluorine atoms is the reason for very low cohesive forces between fluorocarbon segments. Moreover, perfluorocarbons are known to be inert to biological systems, which allows for a diversity of biomedical applications. [1-7]

The weak intermolecular cohesion is one of the unique physical characteristics of fluorocarbons. It makes the solubility of respiratory gases very high.[2] Therefore, perfluorocarbons enriched with oxygen could help patients with acute respiratory distress syndrome (ARDS) continue breathing.[8-9] They have also potential for lung surfactant replacement.[10-12] To date, several studies have shown how fluorocarbons interact with interfaces. For example, fluorocarbon gases reduce the tension at the air/water interface by 2-5 mN/m, suggesting their adsorption.[13] More recently, we reported that perfluorohexane gas facilitates the displacement of albumin by phospholipids,[14] suggesting that a fluorocarbon gas can potentially be used to improve the therapeutic treatment of ARDS patients as it allows-phospholipids to reach the alveolar surface by removing the serum proteins.

Another unique characteristic of perfluorocarbons is their extremely low solubility to water, the solubility limits of perfluorohexane is 2.7×10^{-4} mol/m^3, which is two orders of magnitude lower than the water solubility of nitrogen or oxygen (0.48 mol/m^3). [15-16] This property makes microbubbles of perfluorocarbon vapor attractive for ultrasonic image diagnostics.[17] In general, microbubbles used in sonographic imaging suffer from the collapse of bubbles due to the dissolution of standard gases into water.[17-18] Owing to their extremely poor water solubility, perfluorocarbon gases are expected to significantly increase the life time of microbubbles.[19-20] However, the microbubbles of perfluorocarbon gas alone are not stable enough in physiological fluids. They need to be further stabilized by coating the vapor/water interface by surfactant molecules.[17] Perfluorohexane was found to exert a co-surfactant role with regards to phospholipids forming monolayers at the gas/water interface.[21].

Promising candidates as bubble shell components are semifluorinated alkanes $C_nF_{2n+1}C_mH_{2m+1}$ (*FnHm* diblocks). Previous studies showed their capability to stabilize phospholipid vesicles [22-23] as well as fluorocarbon-in-water emulsions.[24] At the air/water interface, *FnHm* molecules form highly monodisperse domains with the size of 28 – 34 nm.[25] Recently, we employed grazing incidence small angle X-ray scattering (GISAXS) and demonstrated that these compounds spontaneously self-assemble into hemispherical domains taking hexagonal lattices.[25] The precise calculation of form and structure factors revealed that these domains are highly correlated, and their size and correlation can be fine-adjusted by varying the length of the hydrocarbon and fluorocarbon segments.[25] Moreover, we found that such films of *FnHm* at the air/water interface form physical gels even at 0 mN/m surface pressure due to the strong dipole repulsion between the CF_3 terminals and the CF_2-CH_2 junction, which seems promising for the stabilization of fluorocarbon microbubbles.[26]

A key question in the context of using semifluorinated alkanes as shell components in fluorocarbon gas-stabilized microbubbles was if the presence of the fluorocarbon gas affects the structure and mechanical properties of the arrays of self-assembled domains of diblocks. It is conceivable that small fluorocarbon molecules can either penetrate into the domains or adsorb to the spaces between domains. Such a possibility is

comforted by the fact that the tightly packed fluorocarbon segments are exposed to the gas phase.[3, 27-28] Extending our study at the air/water interface, we therefore investigated the self-assembly and the interface mechanics of *FnHm* diblocks in an atmosphere enriched with perfluorohexane (PFH) by the combination of dilational rheology and GISAXS. Both series of experiments were performed by using custom made, gas-tight film balance systems that enable to saturate the atmosphere with PFH. By the systematic variation of fluorocarbon segment lengths, we elucidated how molecular structures influence the static ordering and dynamic viscoelasticity of the *FnHm* domains in a PFH-enriched atmosphere.

Materials and Methods

Materials

The compounds tested in this study, *F*8*H*16, *F*8*H*18, *F*8*H*20, *F*10*H*16, *F*12*H*16, were synthesized according to ref. [29]. They were purified by repeated crystallizations with methanol. Throughout the study, double distilled water (MilliQ, Molsheim, France) with a specific resistance $\rho > 18$ MΩ was used.

Pressure-Area Isotherms, Interfacial Dilational Rheology

The pressure-area isotherm and interfacial dilational rheology experiments of the *FnHm* Langmuir monolayers were performed using a gas-tight Langmuir film balance with two movable barriers (KSV-Nima, Biolin Scientific, Gothenburg, Sweden) at room temperature (T = 293 K) (Fig. S1A). A 40 µL portion of *FnHm* solution (2 mM in $CHCl_3$) was deposited on the water subphase. For the experiments in a PFH-enriched atmosphere, a flow of N_2 gas was led through three subsequent washing bottles filled with liquid PFH into the gas-tight box of the film balance. Since the saturation of PFH was accompanied by an increase in surface pressure to 2.5 - 3 mN/m (Fig. S1B), the surface pressure was manually set to 0 mN/m prior to the compression. Once the system reached the equilibrium, the pressure-area isotherm was recorded by compression of the film at a speed of 3.75 cm^2/min. For the dilational rheology experiments, the monolayer was compressed to π = 5 mN/m, and the barrier positions were sinusoidally oscillated with a relative strain amplitude of $u_0 = \frac{\Delta A}{A_0} = 0.01$. The strain frequency was scanned between 1 and 150 mHz. Both the area per molecule $A(t)$ and surface pressure $\pi(t)$ were recorded over time. Throughout this study, we observed no distinct drop of the surface pressure confirming that no material was lost into the subphase during the measurements.

The elastic and viscous moduli E' and E'' can be calculated by

$$E^* = E' + iE'' = \frac{\pi_1}{u_0}\cos\varphi + i\frac{\pi_1}{u_0}\sin\varphi \qquad (1)$$

Where π_1 is the amplitude of the surface pressure oscillation and φ is the phase shift between area and surface pressure.

Grazing Incidence Small-Angle X-ray Scattering (GISAXS)

GISAXS experiments were performed at ID10 beam line of European Synchrotron Radiation Facility (ESRF, Grenoble, France). A gas-tight film balance filled with either He or PFH-enriched atmosphere was used for the

preparation of *FnHm* monolayers. The monolayer was compressed to the surface pressure of 5 mN/m, and a monochromatic X-ray beam (22 keV) impinged on the interface at an incidence angle of 0.045°, which is slightly lower than the critical angle of total external reflection. The intensity of scattering signal was detected by using a 2D-pixel detector. Fig. S2 shows the scattering geometry of the GISAXS experiment. The scattering signals collected by the detector were translated into a reciprocal space map by:

$$q = \begin{pmatrix} q_x \\ q_y \\ q_z \end{pmatrix} = \frac{2\pi}{\lambda} \begin{pmatrix} \cos(\alpha_f)\cos(2\theta) - \cos(\alpha_i) \\ \cos(\alpha_f)\sin(2\theta) \\ \sin(\alpha_f) + \sin(\alpha_i) \end{pmatrix}, \quad (2)$$

where α_i is the incidence angle and θ and α_i are the angles of the scattered beam (Fig S2). As $q_x \ll q_y$, the scattering signal parallel to the interface is $q_{\parallel} \approx q_y$. To obtain the 1D scattering profile along q_y, the scattering intensity was averaged over $q_z = (1.1 \pm 0.1)$ nm^{-1}. The experimental GISAXS data were analyzed using the FitGISAXS software [30]. The data were treated within the framework of distorted wave Born approximation by applying the implemented functions for monodisperse oblate hemispheroids arranged in a hexagonal paracrystal. The structure factors $S(q_y)$ and form factors $F(q_y)$ were obtained by optimizing the background intensity, scaling factor A, diameter D, height H, and lattice constant L. Finally, the best fit was achieved by floating all parameters.

Results and Discussion

Linear Dilational Viscoelasticity

Fig. 1A shows typical pressure-area isotherms of *F*8*H*16 measured in air and in a PFH-enriched atmosphere. In the presence of PFH, the onset of the increase in surface pressure appeared at a larger area per molecule ($A \approx 36$ Å^2), while the surface pressure increase in air was observed at $A \approx 33$ Å^2. This suggests the adsorption of PFH molecules at the air/water interface (Fig. S1). Actually, as shown in Fig. 1B, the lateral compressibility of the monolayer in PFH atmosphere at the surface pressure of $\pi = 5$ mN/m, $\kappa^{-1}_{F8H16,\mathrm{PFH}} = = -\frac{1}{A}\left(\frac{\partial A}{\partial \pi}\right)_T = 11.3$ m/N, is distinctly higher compared to the value in air $\kappa^{-1}_{F8H16,\mathrm{air}} = 7.4$ m/N. Moreover, the collapse pressure of the *F*8*H*16 monolayer in PFH-enriched atmosphere (≈ 9 mN/m) was lower than that in air (≈ 11 mN/m). The same tendency was also observed for all the other *FnHm* derivatives (Fig. S3, Fig. S4), suggesting that some PFH molecules adsorbing at the air/water interface are intercalated into the *FnHm* monolayers.

Fig. 2A represents the change in surface pressure ($\pi(t)$, black symbols) of a *F*8*H*16 monolayer measured under oscillatory change in the area per molecule $A(t)$ in a PFH-enriched atmosphere at a strain frequency of $f = 100$ mHz and strain amplitude of $u_0 = 0.01$. The global shape of the response function $\pi(t)$ showed a distinct deviation from an ideal sinusoidal function, indicating that the viscoelastic response of a *F*8*H*16 monolayer is nonlinear. Thus, the response function was fitted by a Fourier series expansion

$$\pi(t) = \pi_0 + \sum_{k=1}^{n} \pi_k \sin(k\omega t + \varphi_{\pi k}), \quad (3)$$

where π_k is the amplitude of mode k and $\varphi_{\pi k}$ the corresponding phase shift. As shown in Fig. S5 we confirmed that the fitting up to the 5th mode was sufficient.

In the first step, we focus on the linear contribution and thus analyze only the first mode of the Fourier series expansion. As presented in Fig. S6, the phase separation between stress and strain exhibited a minor increase from $\varphi \approx 0.2$ to 0.6 following the increase in the strain frequency from $f = 1$ mHz to 150 mHz. The fact that the phase shift is well below π/2, indicates that the *F*8*H*16 monolayer is predominantly elastic.

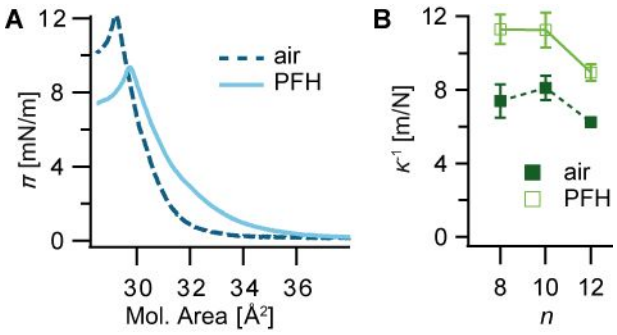

Fig. 1: (A) Pressure-area-isotherms of *F*8*H*16 in air (dashed) and PFH-enriched atmosphere (solid) measured at 20°C with a compression speed of 3.75 cm²/min. (B) The lateral compressibility calculated from the isotherms of all measured *FnH*16 diblocks. The lines are to guide the eye.

Based on the finding, we analyzed the data using a simple Kelvin-Voigt model suited for elastic systems:

$$\sigma = g\epsilon + \eta\frac{d}{dt}\epsilon. \qquad (4)$$

σ is the stress, ϵ the strain, g the spring constant, and η the viscosity. As in our case both stress and strain are oscillating, the elastic and viscous modulus of the Kelvin-Voigt model result in $E' = g$ and $E'' = 2\pi f\eta$, respectively.[31]

Fig. 2B shows the elastic modulus E' (triangles) and the viscous modulus E'' (squares) of *F*8*H*16 monolayers plotted as a function of strain frequency. The results in air are presented with solid symbols, while the data points from the experiments in PFH-enriched atmosphere are shown with open symbols. We observed that *F*8*H*16 monolayers are predominantly elastic, $E' > E''$. The elastic modulus E' is independent from the frequency, while the E'' increases linearly with the frequency. The solid lines correspond to the fitting results, yielding a spring constant of $g_{F8H16,\mathrm{air}} = (128.8 \pm 1.4)$ mN/m and an interfacial viscosity of $\eta_{F8H16,\mathrm{air}} = (20.8 \pm 3.9)$ μN·s/m. Both E' and E'' exhibited the same tendency in PFH-enriched atmosphere (Fig. 2B, open symbols). The elastic modulus E' is almost independent from frequency, yielding a spring constant that is about 25% less compared to the corresponding value in air, $g_{F8H16,\mathrm{PFH}} = (96.8 \pm 2.6)$ mN/m. On the other hand, the viscous modulus shows a linear increase with the frequency, yielding a slightly higher 2D viscosity $\eta_{F8H16,\mathrm{PFH}} = (27.1 \pm 3.8)$ μN·s/m.

In the next step, the influence of the fluorocarbon segment length was investigated. Fig. 2C presents the comparison of spring constant g (triangles) and interfacial viscosity η (circles) of *F*8*H*16, *F*10*H*16, and *F*12*H*16, measured in air (solid symbols) and in PFH-enriched atmosphere (open symbols). In air, the spring constant showed no distinct dependence on the length of fluorocarbon segments, $g_{FnH16,\mathrm{air}} \approx 130$ mN/m. On the other

hand, the interfacial viscosity exhibited a monotonic increase from $\eta_{F8H16,air} = (20.8 \pm 3.9)$ μN·s/m to $\eta_{F12H16,air} = (34.6 \pm 2.9)$ μN·s/m. In the PFH-enriched atmosphere (open symbols), E' and E'' exhibited the same trend, confirming that both *F*10*H*16 and *F*12*H*16 also form 2D gels (Fig. S3). Moreover, both g and η showed no dependence on fluorocarbon segment lengths; $g_{FnH16,\ PFH} \approx 105$ mN/m and $\eta_{FnH16,PFH} \approx 27$ μN·s/m. A same tendency was observed for diblocks with longer hydrocarbon chains *F*8*H*18 and *F*8*H*20 (Fig. S4).

Compared to other surfactants and block copolymers, the dilational elastic moduli of *FnH*16 monolayers are by a factor of 4 larger.[32-35] For example, the spring constant of the lipid dipalmitoylphosphatidylcholine (DPPC) was $g_{DPPC} \approx 30$ mN/m.[35] Particularly, it is remarkable that both the strain amplitude ($u_0 = 0.01$) and surface pressure ($\pi = 5$ mN/m) used in our experiments are much lower than the typical conditions for the dilational rheology experiments, such as $u_0 = 0.03 - 0.2$ and $\pi = 17.7$ mN/m for the DPPC monolayer [35]. The high elastic moduli can be attributed to the strong dipole repulsions between *FnH*16 domains originating from the CF_3 termini. [31, 36-37] The contribution from the dipole moments of the CH_3 termini should be minor, since they are in contact with, or immersed into the water phase with a high dielectric constant, $\varepsilon_r = 80$.[37]

Since *FnH*16 domains expose the fluorocarbon segments to the atmosphere, PFH molecules are either intercalated into the fluorocarbon segments of *FnH*16 domains or adsorbed on the free water surface between the domains. The pressure-area isotherms (Fig. 1A, Fig. S3 and Fig. S4) actually reveal that the lateral compressibilities of *FnH*16 monolayers in the PFH-enriched atmosphere were higher than those in air. Fig. S1B also suggested that PFH molecules are adsorbed at the air water interface, resulting in a slight increase in the surface pressure ($\Delta\pi = 2.5 - 3$ mN/m). Thus, the decrease in the elastic modulus E' (Fig. 2B) and the spring constant g (Fig. 2C) can be correlated to the increase in the lateral compressibility and the decrease in inter-domain repulsions.

The interface viscosity values of *FnH*16 monolayers, $\eta_{FnH16} \approx 21 - 35$ μN·s/m, are by a factor of 100 lower compared to that of surfactants such as $\eta_{DPPC} \approx 20$ mN·s/m.[35] The significantly low energy dissipation through the periodic compression-expansion cycles suggests that the friction between the diblock monolayer and the water subphase is very low. It should be noted that *FnH*16 molecules possess no hydrophilic moieties immersed into the water subphase, which is completely different from most surfactant molecules with hydrophilic head groups. [32, 35]

In air, the elongation of the fluorocarbon segments from $n = 8$ to 10 leads to an increase in the interfacial viscosity, $\eta_{F12H16,air}/\eta_{F8H16,air} \approx 1.7$, which can be explained by an increase in the frictional coupling between *FnH*16 domains due to the increase in the contact to the neighbors. Intriguingly, the interface viscosity became independent from the fluorocarbon segment length in the PFH-enriched atmosphere ($\eta_{FnH16,PFH} \approx 27$ μN·s/m), suggesting that the cohesion between fluorocarbon segments is screened by PFH molecules.

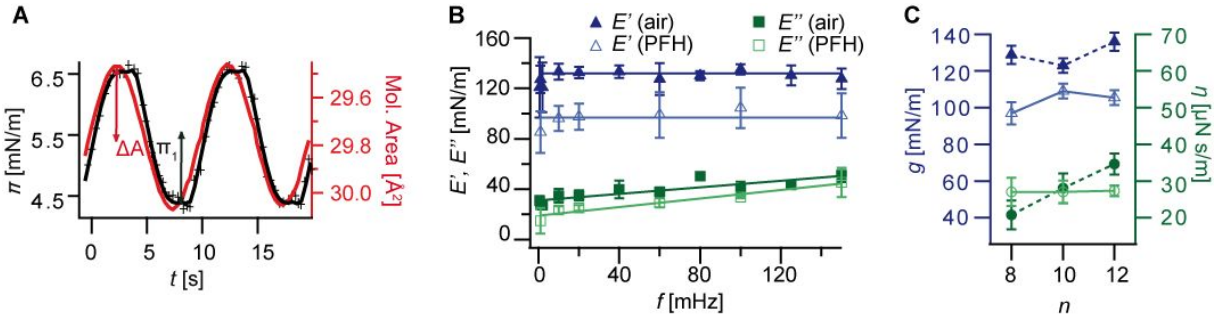

Fig. 2: (A) The applied strain $A(t)$ (red) and the recorded stress response $\pi(t)$ (black symbols) of a F8H16 monolayer in a PFH-enriched atmosphere. The experiment was performed at a strain amplitude of $u_0 = 0.01$ and frequency of $f = 100$ mHz. The black line is the fit with a Fourier series expansion up to the 5th mode. (B) Dilational elastic modulus E' (blue triangles) and viscous modulus E'' (green squares) measured with respect to the frequency for *F*8*H*16 in air (solid symbols) and in a PFH-enriched atmosphere (open symbols). The solid lines are the fits with the Kelvin-Voigt model. (C) Spring constant g (blue) and interface viscosity η (green) of *FnH*16 monolayers obtained from the Kelvin-Voigt model, plotted as a function of fluorocarbon segment length n. The lines are to guide the eye. All data points show the mean values from at least three independent measurements, and the error bars represent the standard deviation.

Nonlinear Viscoelasticity

As presented in Fig. 2A, the global shape of the response function of a *F*8*H*16 monolayer exhibits a clear deviation from the ideal linear response, which can be characterized by the flattened region. This nonlinear behavior is also clearly visible from the Lissajou plots tracing the surface pressure versus the area, which significantly deviate from a perfect ellipse (Fig. S7). Fig. 3A shows the Fourier spectrum of *F*8*H*16 in air (black) and PFH-enriched atmosphere (grey). For both cases, the peaks of the first and third modes seem dominant. Since the percentage of the i-th mode amplitude (π_i) normalized by the first Fourier mode π_1 plotted as a function of strain frequency f (Fig. S10), we plotted the normalized intensity averaged over frequency as a function of the Fourier mode m (Fig. 3B). The amplitude of the third mode (π_3) is ~ 9 % of the first mode (π_1). The fraction of the second and fifth modes are ~ 3 %, which is close to the noise level (2 %). We did not observe any difference between the Fourier spectra and the mode fractions calculated from the experimental data measured in air and the PFH-enriched atmosphere. To further assess the degree of nonlinearity, we calculated the total harmonic distortion (THD):

$$THD = \frac{1}{\pi_1}\sqrt{\sum_{k=2}^{n}\pi_k^2}, \qquad (5)$$

where π_k is the amplitude of the k-th Fourier mode. As the Fourier amplitude is independent of the frequency, we compared the mean THD for every *FnH*16 diblock system in air and PFH-enriched atmosphere (Fig. 3C). The values obtained in air are $THD_{F8H16,air} = (10.7 \pm 0.9)$ %, $THD_{F10H16,air} = (10.3 \pm 0.5)$ % and $THD_{F12H16,air} = (11.8 \pm 0.5)$ %. The THD values of the PFH-enriched atmosphere were actually almost identical to those in air, irrespective of the fluorocarbon segment length and also hydrocarbon segment length (Fig. S4). The fact that PFH only affects the first mode of the Fourier spectrum but not the higher modes suggests that the intercalation or adsorption of PFH does not modulate the nonlinear coupling between *FnH*16 domains.

The emergence of nonlinearity from the third mode originates from the elasticity of the system, because a nonlinear elastic component should be odd under reflection due to mirror symmetry. This can be described by an extended nonlinear Kelvin-Voigt model with an additional spring constant *g'*:

$$\pi(t) \propto g\epsilon + g'\epsilon^3 + \eta\frac{\partial\epsilon}{\partial t}. \qquad (6)$$

In our system, $g' \approx 0.9g$ (Fig. 3B). Within the framework of Landau theory, the transition between diluted and condensed states of *FnH*16 domains can be classified as a first order phase transition, since the Lissajou plots (Fig. S7) imply that the lateral compressibility of the system is $\kappa^{-1} = -\frac{1}{A}\left(\frac{\partial A}{\partial \pi}\right)_T \approx \infty$. We recently investigated the dilational rheology of the monolayers of fluorocarbon/hydrocarbon tetrablocks di(*FnHm*) ($(C_{10}F_{21}CH_2)(C_{m\text{-}2}H_{2m\text{-}3})CH\text{-}CH(C_{10}F_{20}CH_2)(C_{m\text{-}2}H_{2m\text{-}3})$, m = 16, 18, 20) in air, and observed the emergence of the nonlinearity, too.[31]

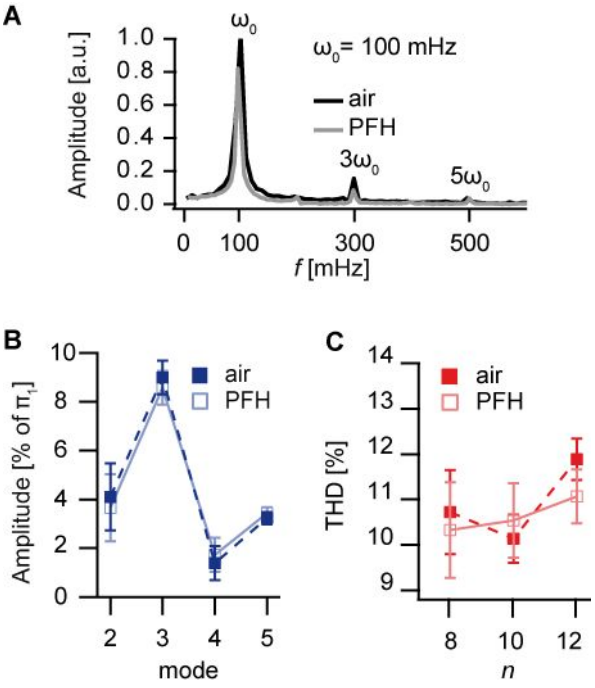

Fig. 3: (A) Fourier spectrum of the response function of *F*8*H*16 recorded at f = 100 mHz in air (black) and PFH atmosphere (grey). (B) Fractions of the i-th Fourier mode amplitude π_i with respect to the first mode π_1, plotted as a function of the strain frequency f. Filled symbols represent air, open symbols PFH atmosphere. (C) THD values of the various *FnH*16 diblocks as a function of the fluorocarbon segment length n. Each data point corresponds to the mean value and the standard deviation, calculated from more than three independent measurements. The lines in (B) and (C) are given to guide the eye.

GISAXS

To obtain more information about the influence of PFH gas on the structure and correlation of *FnH*16 domains, we performed GISAXS measurements in a PFH-enriched atmosphere and compared the results with the data we previously measured in air.[25] Fig. 4A shows the scattering signal of a *F*8*H*16 monolayer in the PFH atmosphere at a surface pressure of 5 mN/m, presented in a 2D reciprocal space coordinate system. The intensity profile

along q_y was obtained by integrating the signal between q_z = 1.0 and 1.2 nm^{-1} (Fig. 3B). The intensity $I(q_y)$ is given by

$$I(q_y) = A \times |F(q_y)|^2 \times S(q_y), \quad (7)$$

where A is a scaling factor, $F(q_y)$ the form factor and $S(q_y)$ the structure factor. $I(q)$, $|F(q)|^2$ and $S(q)$ are shown in red, blue and green lines in Fig. 4B, respectively. The form factor reflects the shape and the size of the domains, whereas the structure factor provides information about the lateral organization. For *FnH*16 domains in PFH-enriched atmosphere, we applied the form factor $F(q_y)$ of oblate hemispheroids with diameter Φ and height H (Eq. S9) and $S(q_y)$ of a 2D hexagonal paracrystal lattice with a lattice parameter L (Eq. S10). This was the same model as the one used for the analysis of the GISAXS data in air. The fact that the best fit (Fig. 4B, red line) could well represent the experimental data implies that the PFH molecules in the gas phase do not cause a coalescence or deformation of the *FnHm* domains. The structure factor $S(q_y)$ is the Fourier transformation of the pair correlation function in real space $g(r)$. Thus, taking the width of the structure factor peak δq_y, the correlation length ξ is given by $\xi = 2\pi^2/\delta q_y$ within the framework of the short range order model.[38]

In Fig. 4C, the diameter Φ (black, solid symbols) was plotted as a function of the fluorocarbon segment length n. The mean diameter of *F*8*H*16 domains was comparable to that of *F*10*H*16 domains, $\Phi_{F8H16,\mathrm{PFH}} \approx \Phi_{F10H16,\mathrm{PFH}} \approx 29$ nm. The domain size of *F*12*H*16 domains was distinctly larger, $\Phi_{F12H16,\mathrm{PFH}}$ = 32 nm. The lattice parameter L calculated from the structure factor of each system was comparable to the corresponding Φ, such as L_{F8H16} = (28.6 ± 5.2) nm, indicating that *FnH*16 domains form tightly packed hexagonal lattices. The correlation length (Fig. 3A, red) exhibited a monotonic increase from ξ_{F8H16} = 330 nm to ξ_{F12H16} = 750 nm according to the elongation of fluorocarbon segments. This denotes that the inter-domain correlation between *FnH*16 domains could reach a distance that is 12 - 28 times longer than the distance to the nearest neighbors. Such a strong, long-range inter-domain correlation can be attributed to the strong dipole repulsions induced by CF_3 termini and CF_2-CH_2 bond.

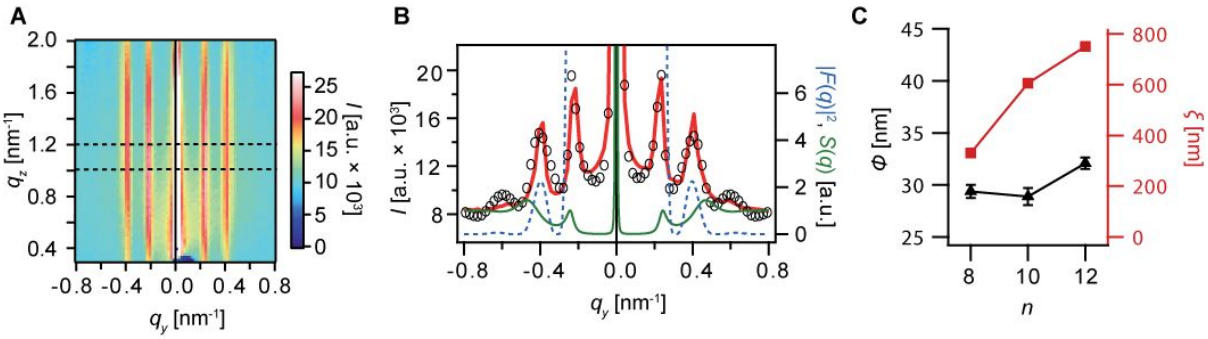

Fig. 4: (A) GISAXS signal from a *F*8*H*16 monolayer in a PFH-enriched atmosphere measured at 5 mN/m, plotted in 2D reciprocal coordinates. (B) Intensity profile along q_y integrated between q_z = 1.0 and 1.2 nm^{-1}, indicated by two dashed lines in panel (A). The red line represents the fitted intensity, including the structure factor (green line) and the form factor (blue line). (C) Calculated diameter Φ (black solid symbols) and the correlation length ξ (red symbols) of *FnH*16 domains in PFH-enriched atmosphere, plotted as a function of fluorocarbon segment length n. The lines are given to guide the eye.

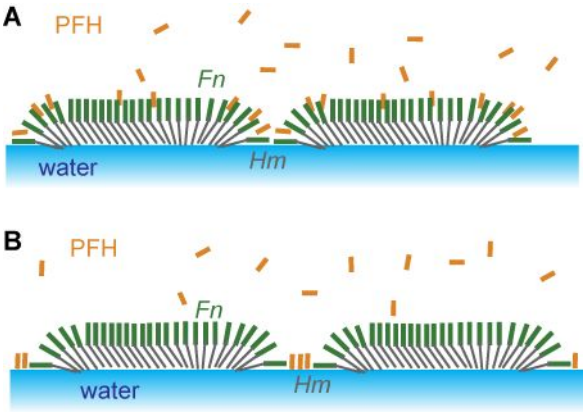

Fig. 5: Two possible scenarios for the interaction between PFH and *FnH*16 domains; (A) intercalation into the fluorocarbon region of *FnH*16 domains and (B) adsorption to the spaces between *FnH*16 domains.

The corresponding values in air extracted from our previous account [25] are presented in Table S11 for comparison. It is remarkable that the enrichment of the gas phase with PFH barely influences the shape, size, and lateral correlation of *FnH*16 domains. The fact that the domain size remained intact clearly indicates that the intercalation of PFH molecules into the fluorocarbon region of the domains is not likely, because such a scenario should result in a "swelling" of the domains (Fig. 5A). Therefore, the adsorption of PFH molecules to the spaces between the domains seems more plausible (Fig. 5B). Actually, as presented in Fig. 1A, the difference between the area per molecule of *F*8*H*16 at π = 5 mN/m in PFH-enriched atmosphere ($A_{F8H16,\mathrm{PFH}}$ = 30.9 Å^2) and in air ($A_{F8H16,\mathrm{air}}$ = 30.3 Å^2) is very minor, which seems to agree well with the GISAXS data showing no major differences. However, when we compare the lateral compressibility measured at π = 5 mN/m, the compressibility in the PFH-enriched atmosphere $\kappa^{-1}{}_{F8H16,\mathrm{PFH}} = -\frac{1}{A}\left(\frac{\partial A}{\partial \pi}\right)_T$ = 11.3 m/N is 50 % larger than that in air, $\kappa^{-1}{}_{F8H16,\mathrm{air}}$ = 7.4 m/N (Fig. 1B). Therefore, it is plausible that the significant retardation of the lateral compressibility and hence the inter-domain repulsion caused by the adsorption of PFH molecules to the spaces between the domains results in a distinct decrease in the elastic modulus E' and spring constant g (Fig. 2A). On the other hand, the interfacial viscosity η originates from the friction at the domain/water interface as well as the frictional coupling between individual domains. The fact that the interfacial viscosity is independent from the fluorocarbon segment length (Fig. 2B) suggests that the PFH molecules adsorbed to the gaps between the *FnH*16 domains do not influence the friction at the domain/water interface or the interdomain friction. Intriguingly, the stress response function exhibited no hysteresis after several compression/expansion cycles, suggesting that the adsorption and desorption of PFH molecules are weak due to the extremely hydrophobic nature of fluorocarbon molecules. Indeed, the compression of the blank subphase in PFH-enriched atmosphere did not cause any remarkable increase in the surface pressure (Fig. S12). This might explain our results indicating that PFH molecules enriched in the gas phase barely influence the nonlinearity of the response function (THD). This suggests that the self-assembled domains of *FnH*16*m* prevent the intercalation of PFH molecules into the fluorocarbon region, which seems to be in line with the formation of 2D gels by these nanodomains at the gas/water interface.[26]

Conclusions

Microbubbles enriched with fluorocarbon gas molecules are promising candidates as contrast agent for sonographic imaging, because the solubility of fluorocarbon into water is extremely poor. Semifluorinated alkanes, $C_nF_{2n+1}C_mH_{2m+1}$, (*FnHm* diblocks), are self-assembled into highly uniform, strongly correlated domains that form two-dimensional physical gels at the air/water interfaces. However, little is known about how the presence of a fluorocarbon gas would influence the structure and mechanics of *FnHm* monolayers.

In this study, we measured dilational rheology and grazing incidence small-angle X-ray scattering (GISAXS) of *FnHm* diblocks in an atmosphere enriched with perfluorohexane (PFH), using gas-tight Langmuir film balance systems. The pressure-area isotherms of *FnHm* monolayers measured in a PFH-enriched atmosphere showed the onset of surface pressure increase at larger mean molecular areas compared to the curves recorded in air (Fig. 1A). As shown in Fig. 1B, the lateral compression modulus at π = 5 mN/m in the PFH-enriched atmosphere, $\kappa^{-1}{}_{F8H16,\mathrm{PFH}} = = -\frac{1}{A}\left(\frac{\partial A}{\partial \pi}\right)_T$ = 11.3 m/N, was distinctly higher than that in air $\kappa^{-1}{}_{F8H16,\mathrm{air}}$ = 7.4 m/N. The viscoelastic properties of *FnHm* monolayers were measured by monitoring the surface pressure $\pi(t)$ under the sinusoidal oscillation of the surface area. Here the strain amplitude was kept at $u_0 = 0.01$ to avoid the collapse of monolayers, while the frequency of strain was varied between 1 and 150 mHz. Since the global shape of the response function, i.e. the change in surface pressure $\pi(t)$, measured under oscillatory change of the area per molecule $A(t)$ exhibited a clear nonlinearity, we fitted it by a Fourier series expansion up to the 5th mode (Fig. 2A). In the first step, we focused only on the first Fourier mode and thus the linear part of the viscoelastic response, and fitted the data with the Kelvin-Voigt model. The results presented in Fig. 2B indicated that *FnH*16 monolayers were predominantly elastic ($E' > E''$). The elastic modulus of *FnH*16 diblocks was about 4 times larger than the typical levels of other surfactants, which can be attributed to the strong dipole repulsions between *FnH*16 domains originating from CF_3 termini and CF_2−CH_2 bonds. Intriguingly, the spring constants g in PFH-enriched atmosphere were distinctly lower, which can be correlated to the higher lateral compressibility observed in the pressure-area isotherms. The calculated spring constant g showed no dependence on the fluorocarbon segment length both in air and in PFH-enriched atmosphere, while the interfacial viscosity η showed a linear dependence on fluorocarbon segment lengths in air but no dependence in PFH-enriched atmosphere (Fig. 2C). These data imply that PFH molecules screen the friction at the domain/water interface and/or inter-domain frictions. Moreover, we found that the the presence of PFH gases barely influenced the Fourier amplitudes of higher modes and the total harmonic distortion (Fig. 3).

To gain further insights into the structural origin of the modulation of viscoelastic response of *FnH*16 monolayers, we performed GISAXS in a PFH-enriched atmosphere (Fig. 4A) and compared the results with the data obtained in air.[25] To analyze the GISAXS data, we applied the form factor $F(q_y)$ of oblate hemispheroids with diameter Φ and height H and the structure factor $S(q_y)$ of a 2D hexagonal paracrystal lattice with a lattice parameter L (Fig. 4B). We found that the diameter obtained from the form factor and the lattice parameter obtained from the structure factor are almost the same, indicating that the domains are tightly packed into a hexagonal arrangement not only in air but also in the PFH-enriched atmosphere. The correlation length calculated from the peak width of the structure factor indicated that the correlation between *FnH*16 domains can reach over a distance that is 12 – 28 times longer than the domain diameter (Fig. 4C). The quantitative GISAXS data demonstrate that the shape, size, and lateral correlation of *FnH*16 domains remain almost intact, denoting that PFH molecules do not intercalate into the fluorocarbon region of domains but weakly adsorb to the gaps between *FnH*16 domains. This could explain the clear decrease in the elastic modulus or spring constant in terms

of the retardation of dipole repulsions between the *FnH*16 domains. Nevertheless, the adsorption of PFH to the air/water interface seems to be weak, because the stress response function exhibited no hysteresis. The obtained results demonstrate how subtle changes in the molecular structures can influence the shape, size and lateral correlation of mesoscopic domains of self-assembled small molecules at the air/water interface. Quantitative GISAXS allows the precise determination of the size and order of 30 nm large objects floating on the water surface that are not visible by optical microscopy, and the combination with dilational rheology enables to correlate the structural order and the interface mechanics. Such a strategy can be used for the fine adjustment of molecular level structures to optimize the mechanical properties of membranes, bubbles, and emulsions.

Acknowledgements

We thank ESRF for the synchrotron radiation beam time. We thank the French Research Agency (grant ANR-14-CE35-0028-01 to M.P.K., including a PhD scholarship for X.L.), the German Science Foundation (DFG Ta259/12 to M.T.), and the INTERREG V Upper Rhine Program (« Transcending borders with every project ») and by the Swiss Confederation and the Swiss cantons of Aargau, Basel-Landschaft and Basel-Stadt (NANOTRANSMED to M.P.K. and M.T.). S.M. thanks the Konrad-Adenauer Foundation for the doctoral fellowship, and W.A. the Alexander von Humboldt Foundation for the postdoctoral fellowship. M.T. is thankful to Nakatani Foundation for support.

References

1. Lemal, D. M., Perspective on fluorocarbon chemistry. *The Journal of organic chemistry* **2004,** *69* (1), 1-11.

2. Krafft, M. P.; Riess, J. G., Perfluorocarbons: Life sciences and biomedical uses Dedicated to the memory of Professor Guy Ourisson, a true RENAISSANCE man. *Journal of Polymer Science Part A: Polymer Chemistry* **2007,** *45* (7), 1185-1198.

3. Krafft, M. P.; Riess, J. G., Chemistry, physical chemistry and uses of molecular fluorocarbon-hydrocarbon diblocks, triblocks and related compounds - Unique apolar components for self-assembled colloid and interface engineering. *Chem. Rev.* **2009,** *109*, 1714-1792.

4. Falde, E. J.; Yohe, S. T.; Colson, Y. L.; Grinstaff, M. W., Superhydrophobic materials for biomedical applications. *Biomaterials* **2016,** *104*, 87-103.

5. Sheeran, P. S.; Luois, S. H.; Mullin, L. B.; Matsunaga, T. O.; Dayton, P. A., Design of ultrasonically-activatable nanoparticles using low boiling point perfluorocarbons. *Biomaterials* **2012,** *33* (11), 3262-3269.

6. Díaz-López, R.; Tsapis, N.; Fattal, E., Liquid perfluorocarbons as contrast agents for ultrasonography and 19F-MRI. *Pharmaceutical research* **2010,** *27* (1), 1.

7. Song, G.; Liang, C.; Yi, X.; Zhao, Q.; Cheng, L.; Yang, K.; Liu, Z., Perfluorocarbon-Loaded Hollow Bi2Se3 Nanoparticles for Timely Supply of Oxygen under Near-Infrared Light to Enhance the Radiotherapy of Cancer. *Advanced materials* **2016,** *28* (14), 2716-2723.

8. Bleyl, J. U.; Ragaller, M.; Tschö, U.; Regner, M.; Hübler, M.; Kanzow, M.; Vincent, O.; Albrecht, M., Changes in pulmonary function and oxygenation during application of perfluorocarbon vapor in healthy and oleic acid-injured animals. *Critical care medicine* **2002,** *30* (6), 1340-1347.

9. de Abreu, M. G.; Quelhas, A. D.; Spieth, P.; Bräuer, G.; Knels, L.; Kasper, M.; Pino, A. V.; Bleyl, J.-U.; Hübler, M.; Bozza, F., Comparative Effects of Vaporized Perfluorohexane and Partial Liquid Ventilation in Oleic Acid–induced Lung Injury. *The Journal of the American Society of Anesthesiologists* **2006,** *104* (2), 278-289.

10. Krafft, M. P., Overcoming inactivation of the lung surfactant by serum proteins: a potential role for fluorocarbons? *Soft matter* **2015,** *11* (30), 5982-5994.

11. Gerber, F.; Krafft, M. P.; Vandamme, T. F.; Goldmann, M.; Fontaine, P., Fluidization of a dipalmitoyl phosphatidylcholine monolayer by fluorocarbon gases: potential use in lung surfactant therapy. *Biophysical journal* **2006,** *90* (9), 3184-3192.

12. Nakahara, H.; Lee, S.; Krafft, M. P.; Shibata, O., Fluorocarbon-hybrid pulmonary surfactants for replacement therapy-a Langmuir monolayer study. *Langmuir* **2010,** *26* (23), 18256-18265.

13. Chernyshev, V. S.; Skliar, M., Surface tension of water in the presence of perfluorocarbon vapors. *Soft matter* **2014,** *10* (12), 1937-1943.

14. Nguyen, P. N.; Veschgini, M.; Tanaka, M.; Waton, G.; Vandamme, T.; Krafft, M. P., Counteracting the inhibitory effect of proteins towards lung surfactant substitutes: a fluorocarbon gas helps displace albumin at the air/water interface. *Chemical Communications* **2014,** *50* (78), 11576-11579.

15. Haynes, W. M., *CRC Handbook of Chemistry and Physics, 96th Edition*. CRC Press: 2015.

16. Kabalnov, A.; Klein, D.; Pelura, T.; Schutt, E.; Weers, J., Dissolution of multicomponent microbubbles in the bloodstream: 1. Theory. *Ultrasound in medicine & biology* **1998,** *24* (5), 739-749.

17. Krafft, M. P., Fluorine in medical microbubbles–Methodologies implemented for engineering and investigating fluorocarbon-based microbubbles. *Journal of Fluorine Chemistry* **2015,** *177*, 19-28.

18. Paefgen, V.; Doleschel, D.; Kiessling, F., Evolution of contrast agents for ultrasound imaging and ultrasound-mediated drug delivery. *Frontiers in pharmacology* **2015,** *6*, 197.

19. Riess, J. G., Blood substitutes and other potential biomedical applications of fluorinated colloids. *J. Fluor. Chem.* **2002,** *114* (2), 119-126.

20. Szíjjártó, C.; Rossi, S.; Waton, G.; Krafft, M. P., Effects of perfluorocarbon gases on the size and stability characteristics of phospholipid-coated microbubbles: osmotic effect versus interfacial film stabilization. *Langmuir* **2012,** *28* (2), 1182-1189.

21. Nguyen, P. N.; Trinh Dang, T. T.; Waton, G.; Vandamme, T.; Krafft, M. P., A nonpolar, nonamphiphilic molecule can accelerate adsorption of phospholipids and lower their surface tension at the air/water interface. *ChemPhysChem* **2011,** *12* (14), 2646-2652.

22. Ferro, Y.; Krafft, M. P., Incorporation of semi-fluorinated alkanes in the bilayer of small unilamellar vesicles of phosphatidylserine: impact on fusion kinetics. *Biochimica et Biophysica Acta (BBA)-Molecular and Cell Biology of Lipids* **2002,** *1581* (1), 11-20.

23. Schmutz, M.; Michels, B.; Marie, P.; Krafft, M. P., Fluorinated vesicles made from combinations of phospholipids and semifluorinated alkanes. Direct experimental evidence of the location of the semifluorinated alkane within the bilayer. *Langmuir* **2003,** *19* (12), 4889-4894.

24. Marie Bertilla, S.; Thomas, J.-L.; Marie, P.; Krafft, M. P., Cosurfactant effect of a semifluorinated alkane at a fluorocarbon/water interface: impact on the stabilization of fluorocarbon-in-water emulsions. *Langmuir* **2004,** *20* (10), 3920-3924.

25. Veschgini, M.; Abuillan, W.; Inoue, S.; Yamamoto, A.; Mielke, S.; Liu, X.; Konovalov, O.; Krafft, M. P.; Tanaka, M., Size, Shape, and Lateral Correlation of Highly Uniform, Mesoscopic, Self-Assembled Domains of Fluorocarbon–Hydrocarbon Diblocks at the Air/Water Interface: A GISAXS Study. *ChemPhysChem* **2017,** *18* (19), 2791-2798.

26. Veschgini, M.; Habe, T.; Mielke, S.; Inoue, S.; Liu, X.; Krafft, M. P.; Tanaka, M., Existence of Two-Dimensional Physical Gels even at Zero Surface Pressure at the Air/Water Interface: Rheology of Self-Assembled Domains of Small Molecules. *Angewandte Chemie International Edition* **2017,** *56* (41), 12603-12607.

27. Maaloum, M.; Muller, P.; Krafft, M. P., Monodisperse surface micelles of nonpolar amphiphiles in Langmuir monolayers. *Angewandte Chemie* **2002,** *114* (22), 4507-4510.

28. Schwieger, C.; Liu, X.; Krafft, M. P., Self-assembled mesoscopic surface domains of fluorocarbon–hydrocarbon diblocks can form at zero surface pressure: tilting of solid-like hydrocarbon moieties compensates for cross-section mismatch with fluorocarbon moieties. *Physical Chemistry Chemical Physics* **2017,** *19* (35), 23809-23816.

29. Brace, N. O., Syntheses with perfluoroalkyl radicals from perfluoroalkyl iodides. A rapid survey of synthetic possibilities with emphasis on practical applications. Part one: alkenes, alkynes and allylic compounds1. *Journal of fluorine chemistry* **1999,** *93* (1), 1-25.

30. Babonneau, D., FitGISAXS: software package for modelling and analysis of GISAXS data using IGOR Pro. *Journal of Applied Crystallography* **2010,** *43* (4), 929-936.

31. Mielke, S.; Habe, T.; Veschgini, M.; Liu, X.; Yoshikawa, K.; Krafft, M. P.; Tanaka, M., Emergence of Strong Nonlinear Viscoelastic Response of Semifluorinated Alkane Monolayers. *Langmuir* **2018,** *34* (7), 2489-2496.

32. Wantke, K.-D.; Fruhner, H.; Örtegren, J., Surface dilatational properties of mixed sodium dodecyl sulfate/dodecanol solutions. *Colloids Surf., A* **2003,** *221* (1), 185-195.

33. Stubenrauch, C.; Miller, R., Stability of foam films and surface rheology: an oscillating bubble study at low frequencies. *J. Phys. Chem. B* **2004,** *108* (20), 6412-6421.

34. Kim, C.; Yu, H., Surface rheology of monolayers of triblock copolymers of PEO and PPO: surface light scattering studies at the air/water interface. *Langmuir* **2003,** *19* (10), 4460-4464.

35. Vrânceanu, M.; Winkler, K.; Nirschl, H.; Leneweit, G., Surface rheology of monolayers of phospholipids and cholesterol measured with axisymmetric drop shape analysis. *Colloids Surf., A* **2007,** *311* (1-3), 140-153.

36. Seul, M.; Andelman, D., Domain shapes and patterns: the phenomenology of modulated phases. *Science* **1995,** *267* (5197), 476.

37. Schneider, M. F.; Andelman, D.; Tanaka, M., Stripes of partially fluorinated alkyl chains: Dipolar Langmuir monolayers. *J. Chem. Phys.* **2005,** *122* (9), 094717.

38. Schmidbauer, M.; Hanke, M.; Köhler, R., Asymmetric correlation function describing the positional ordering of liquid-phase-epitaxy Si–Ge nanoscale islands. *Physical Review B* **2005,** *71* (11), 115323.